Indian Journal of Chemistry
Vol. 65, February 2026, pp. 164-172
DOI: 10.56042/ijc.v65i2.27626

Green synthesis of zinc oxide nanoparticles: Exploring catalytic and antibacterial potential

N P Patil[a], S D Shinde[a], D S Gaikwad[b], S D Ghatage[c] & K A Undale*[c]

[a] Department of Chemistry, Vivekanand College, (Empowered Autonomous Institute), Kolhapur 416 003, Maharashtra, India

[b] Shikshanmaharshi Dr. Bapuji Salunkhe College, Miraj 416 410, Maharashtra, India

[c] Department of Chemistry, Padmabhushan Dr. Vasantraodada Patil, Mahavidyalay, Tasgaon, Sangali 416 405, Maharashtra, India

E-mail: drkedarundale@gmail.com

Received 16 January 2026; accepted (revised) 3 February 2026

The design a nano-catalytic system by using green route has been a significant challenge to researchers. Recently the biosynthesized metal, and metal oxide nanoparticles are being used as heterocyclic and recyclable catalysts in the area of organic catalysis. Notably, the extract derived from *Thevetia peruviana* (*T. peruviana*) flowers has been employed in Zinc Oxide nanoparticles (ZnO NPs) synthesis. Phytochemicals present in *T. peruviana* flowers act as a stabilizing agent and $ZnSO_4.5H_2O$ is used as a precursor for the synthesis of ZnO NPs. The structural and optical properties of the green synthesized ZnO NPs have been studied using UV–Visible spectrum, Fourier Transform Infrared Spectroscopy (FT-IR), X-ray diffraction (XRD), Field Emission-Scanning Electron Microscopy (FE-SEM), EDX, High Resolution-Transmission Electron Microscope (HR-TEM) and Selected Area Diffraction (SAED). The significant antibacterial activity of ZnO NPs has been checked against pathogenic bacterial strains namely Gram $^{+}$ve bacteria (*Staphylococcus aureus*) and Gram $^{-}$ve bacteria (*Escherichia coli*) and it has been concluded that the ZnO NPs have a good ability to resist microbes. Furthermore, the synthesis of Xanthene with excellent yield using ZnO NPs as a catalyst in aqueous media at room temperature is reported.

Keywords: ZnO NPs, Biosynthesis, *Thevetia peruviana*, Xanthene, Antibacterial activity

Nanotechnology has firmly established itself as an innovative technology, permeating various industrial sectors including chemical, pharmaceutical, mechanical, food processing, and textile industries[1]. Its influence extends into computing, power generation, optics, drug delivery, and environmental sciences[2]. Nanoparticles have revolutionized various fields, and continuous advancements are required to harness their full potential. The US Food and Drug Administration (USFDA) defines nanomaterials (NMs) as substances characterized by having at least one dimension within the approximate range of 1 to 100 nm and demonstrating phenomena that are dependent on their dimensions[3].

Various methods for synthesizing nanoparticles (NPs) are currently being explored, encompassing both physical and chemical approache[4,5]. The chemical methods includes techniques such as hydrothermal sol-gel, solvothermal, sonochemical, electro deposition process, and spray pyrolysis while physical methods include thermal evaporation, pulse laser deposition chemical vapor deposition metal–organic chemical deposition.

In spite of their efficacy, these techniques often carry inherent drawbacks, including high costs, time-intensive procedures, and environmental toxicity. The significance of environmental compatibility becomes apparent in scenarios where it is imperative to sidestep the introduction of harmful byproducts or residual toxicity during the remediation process. Traditional reducing agents, such as sodium citrate, sodium borohydride, and various alcohols, commonly employed in conventional processes, are notorious for their hazardous properties, toxicity, flammability, explosiveness, and resistance to decomposition[6].

Faced with these challenges, researchers are actively exploring alternatives that are safer, non-toxic, and environmentally friendly for the fabrication of nanoparticles. The biosynthesis approach offers a distinct advantage by enabling precise control over the nanoparticle morphology, ensuring a consistent and uniform spherical shape[7,8]. The utilization of plants, bacteria, and microorganisms for the synthesis of transition metal, and metal oxide, nanoparticles, although initiated in the nineteenth century, only gained significant attention in recent decades[9,10].

These natural materials substitute toxic chemicals in the synthesis of metal, metal oxide nanoparticles and nanocomposites, adhering to the principles of green chemistry. Within plants, various active biomolecules like phenols, flavonoids, polyphenolics, and alkaloids are present, exhibiting potential roles as stabilizing, reducing, and capping agents[11].

The synthesis of Zinc Oxide nanoparticles (ZnO NPs) using aqueous extracts from various plant parts, such as roots, leaves, stems, flowers, pods, and fruits, has been extensively documented[12-14]. In these instances, the plant extracts served as biological agents for the fabrication of ZnO NPs. Phytochemicals present in plant parts influencing the size, shape, and surface properties of the synthesized ZnO NPs [15]. Recently, there have been notable and thorough reviews on the biological synthesis of ZnO NPs[16]. A sustainable and eco-friendly approach to synthesizing ZnO NPs not only reduces the environmental impact but also aligns with global efforts to adopt green and clean technologies. This research contributes to the growing field of green nanotechnology, offering an alternative to conventional methods.

The nanoparticles exhibit unique properties and high surface areas, chemical stability, and reusability for multiple runs making them highly effective in promoting various chemical transformations[17]. Their substantial surface area provides numerous active sites, significantly accelerating reaction rates while concurrently minimizing reaction times. Moreover, metal and metal NPs enhance product yields and demonstrate excellent reusability. This capability is particularly valuable in organic synthesis and industrial processes[18]. The numerous publications within the catalysis field affirm that a diverse array of heterogeneous materials satisfy multiple principles of green chemistry when utilized as nanocatalysts[19]. Thus, a wide range of plant-mediated metal and metal oxide nanoparticles play a crucial role as catalysts, finding applications in diverse chemical reactions such as oxidation, reduction, condensation, hydrolysis, coupling, degradation, and organic multicomponent reactions[20,21].

Among the metal and metal nanoparticles, ZnO NPs stand out as versatile inorganic materials with applications spanning energy conservation, textiles, electronics, cosmetics, semiconductors, catalyst and chemical sensing effects[22,23]. ZnO NPs, known for their non-toxic and biocompatible nature, exhibit excellent biomedical properties, including anticancer, anti-inflammatory, and antimicrobial attributes, making them valuable in targeted drug delivery, wound healing, and bioimaging[24].

In a comprehensive exploration of literature, it has been observed that xanthene derivatives are captivated with multifarious biological activities[25-33] including potent antimicrobial, insecticidal, antiviral, antioxidant,t antimalarial, anti-inflammatory, analgesic, antiproliferative activity, anticancer and urease activity, inhibition of trypanothione reductase, bone morphogenetic protein (BMP-2)-targeted osteogenic agents. The expansion of a synthetic route for the synthesis of these biologically active compounds using a facile, environmentally benign and nontoxic catalyst is of enormous significance from the academic as well as industrial points of view.

In the present work, we highlight the utilization of *T. peruviana* flowers, a natural substance as a stabilizing agent to generate crystalline ZnO NPs. Following the synthesis of novel plant-mediated ZnO NPs will be extensively analyzed and characterized using modern techniques. Also we have reported the catalytic activity of biosynthesized zinc oxide nanoparticles to the synthesis of 9-substituted xanthene-1,8-diones. Consequently, we assess the antibacterial efficacy of the green-synthesized ZnO NPs against a spectrum of pathogenic microorganisms.

Experimental Section

Analytic-grade reagents and reactants were used in the experiment without further purification. Flowers of *Thevetia peruviana* (*T. peruviana*) were collected from Kolhapur, Maharashtra, India. The deionized water (DW) was utilized throughout the experiments.

Preparation of *Thevetia peruviana* flowers extract

The flowers of the *T. peruviana* were washed with tap water and then double distilled water to remove the surface impurities. Flowers were dried in the shade, and ground to powder using a grinder. 10 g of *T. peruviana* flowers powder was added into 100 mL of DW and boiled for 45 min at 80°C with magnetic stirring. After cooling, the extract was filtered using filter paper (Whatman No.41) and stored at 4°C for the synthesis of nanoparticles.

Biosynthesis of the ZnO NPs

Here, the biosynthetic method was used to synthesize ZnO NPs. 25 mL of 0.5 M $ZnSO_4.5H_2O$, was added drop-wise into the 25 mL of plant extract for 15 min with continuous stirring at RT and basic *p*H (11) (Ref. 34). The color of the solution was changed from brown to soft greenish, it was indicated that the ZnO NPs were synthesized in that reaction mixture.

The biochemical compounds found in the plant extract was liable for the stabilization of Zn^{2+} metal ions[35]. The reaction mixture was centrifuged and washed with with Deionized water (DI) (3×25 mL) and then ethanol (2×5.0 mL) and dried in an oven at 80°C. This ratio gave best results hence used in the synthesis process. The dried product was calcinated[13] in the muffle furnace at 400°C for 2 hr. The whitish-colored ZnO NPs were obtained and stored for further applications.

Characterization

The biosynthesized ZnO NPs were first characterized by UV-vis absorption spectroscopy (Shimadzu UV-3600, Japan). The reaction mixtures were scanned in the wavelength range between 200 and 800 nm. The crystalline nature of the ZnO NPs synthesized using *T. peruviana* was studied by XRD (AXS-D8 Advance, Bruker Ltd Germany). FT-IR recorded by the Bruker ALPHA to determine the functional groups of the ZnO NPs. FE-SEM Microscopy (MIRAJ 3 TESCAN Ltd., Czech Republic) was used to study the surface morphology of the ZnO NPs. The elements in the samples were probed by EDX spectroscopy accessory to the Philips scanning electron microscopy. The morphological investigation and particle size distribution analysis were carried out using HR-TEM microscopy. The particle size of synthesized ZnO NPs was calculated using ImageJ software. The ^{1}H and ^{13}C NMR spectra are recorded by the 400 MHz Jeol solid state spectrometer in $CDCl_3$ solvent at RT and the use of TMS as an internal standard.

General experimental procedure for the synthesis of xanthene

For the synthesis of xanthene, aldehyde (1.0 mmol), dimedone (2.0 mmol), ZnO NPs (25 mol%) and 5 mL green solvent were mixed thoroughly in an oven-dried Schlenk flask. The reaction mixture was stirred vigorously. The progress of the reaction was monitored by thin-layer chromatography. After consumption of starting materials as determined by TLC analysis, the reaction mixture was extracted with ethyl acetate (3 X 5.0 mL). The solid compound obtained was filtered, dried out, and recrystallized in ethanol to give the pure product. The synthesized compound was confirmed by melting point, ^{1}H and ^{13}C NMR.

Antibacterial susceptibility test

Antibacterial susceptibility tests were carried out against two drug-resistant bacterial strains using the agar disc diffusion method[36]. The two pathogenic drug-resistant bacteria used in the experiment were, *Escherichia coli* (*E.coli*), *S*taphylococcus *aureus* (*S. aureus*). The bacterial broth was consistently distributed on a nutrient agar plate at a density of 1×108CFU mL^{-1}. First of all, the bacterial broth was refreshed using a shaking incubator for 24 hrs at 37°C, 200 rpm. Ampicillin, as a standard antibiotic (10 mg mL^{-1}), and zinc nitrate salt (2 mM) were also added to the test as negative and positive controls, respectively.

Results and Discussion

Characterization of ZnO nanoparticles

UV-visible spectroscopic analysis of ZnO NPs

UV-visible spectroscopic analysis was conducted to confirm the biogenic synthesis of ZnO NPs. For this typical analysis, the sample was dissolved in deionized water. The UV-visible wavelength range was between 200 and 800 nm. The sharp peak obtained at 287 nm confirmed the presence of ZnO NPs in the mixture (Fig. 1). The broad absorption band that ranges towards longer wavelength might be owing to the movement of the electronic cloud on the overall skeleton of the ZnO NPs. The band gap energy (Eg) was determined from the UV-visible spectroscopy data. By using the equation No.1, the optical band gap of the ZnO NPs was found to be 3.75 eV, as shown in Fig. 2.

$$\alpha h\nu = A\,(h\nu - Eg)^{n} \qquad \text{(Eq. No. 1)}$$

Where α is the absorption coefficient, hν represents the energy of the photon, *A* is the proportionality constant and varies with the material, and *n* represents the index.

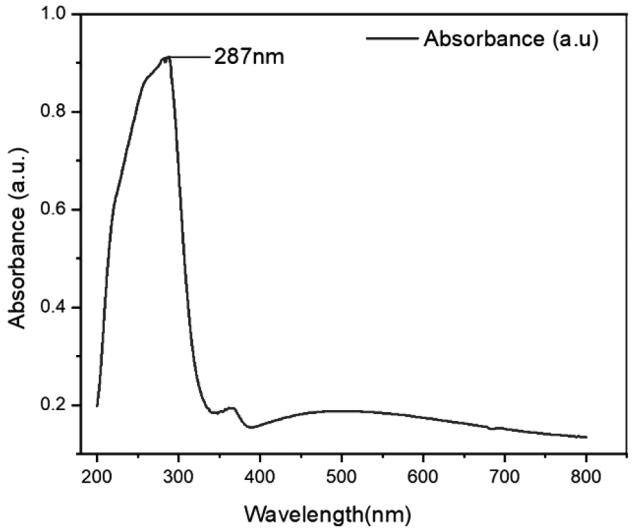

Fig. 1 — UV-visible of biosynthesized ZnO NPs

X-ray diffraction analysis

The crystallinity and crystal phase of the obtained ZnO nanopowder was probed by an X-ray diffraction The XRD pattern for the biogenic synthesized ZnO NPs is shown in Fig. 3 The XRD peaks at 2θ=31.7690, 34.4036, 36.2700, 47.5146, 56.6337, 62.9387, 68.0640, and 69.1230 correspond to the (100), (002), (101), (102), (110), (103), (102), and (201) respectively. The crystal planes and crystal geometry was determined according to JCPDS card no.00-036-1451. The average crystalline size of the ZnO NPs was which was determined by using the Scherrer equation (Eq. No.2).

$$D = K\lambda/(\beta\cos\theta) \qquad \text{(Eq. No. 2)}$$

where D is the crystallite size of the particle, K represents the Scherrer constant, which is equal to 0.9, λ is the wavelength of light used for diffraction (l=1.54 Å), β is the full width at half maximum (FWHM) of the diffraction peak and θ is the angle of reflection. The average size of the ZnO NPs calculated from the XRD pattern was 27.84 nm.

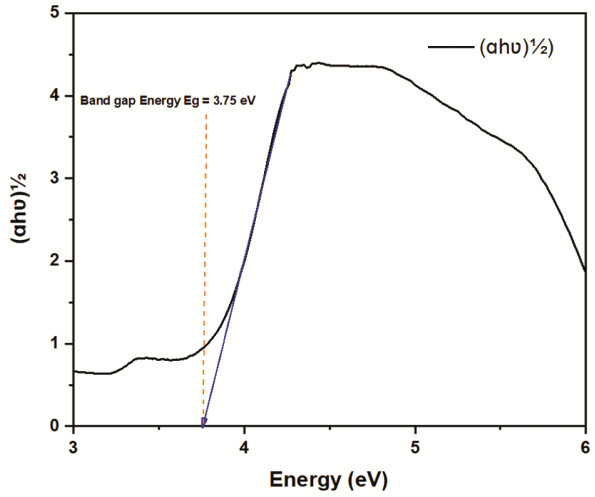

Fig. 2 — Band gap energy of biosynthesized ZnO NPs

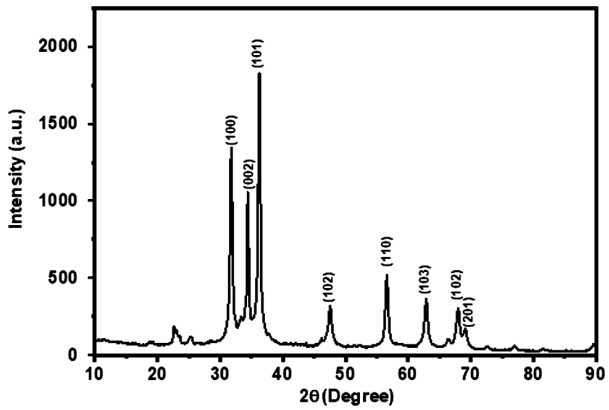

Fig. 3 — XRD diffraction patterns of ZnO NPs

FT-IR analysis

FT-IR spectrum of ZnO NPs is shown in Fig. 4. The IR spectrums evidently have shown the Metal-Oxygen (Zn-O) peaks at 509.43 and 625.53 cm^{-1}. The additional two peaks are at 2372 and 2384 cm^{-1} confirmed the C-H stretching. The peaks were observed at 1572.59 due to C=C stretching frequency and broad peak at 3411.71 cm^{-1} because of the accessible of O-H stretching vibrations[20] and the sharp peak is appeared at 1123.44 cm^{-1} due to C-O stretching.

FE-SEM and EDX analysis of ZnO NPs

For further characterization, the ZnO NPs were analyzed by SEM to observe their morphology and structure. The current study revealed that the ZnO NPs are spherical and nanocrystallites in nature. The electrostatic forces between the biomolecules on the nanoparticle surface causes agglomeration[37] of ZnO NPs as shown in Fig. 5. The EDX was performed to investigate the chemical purity and stoichiometry of the biosynthesized ZnO NPs. The EDX reveals a strong signal at 3keV which is generally shown by metallic ZnO nanocrystals due to surface plasmon resonance[35]. Corresponding EDS mapping of ZnO NPs demonstrated the distribution of O, and Zn elements throughout the ZnO sample. The elemental analysis showed of 40.30%.Zinc and 59.70% of oxygen suggesting that the ZnO nanopowder has good purity and no impurities can be seen. Theoretically expected the stoichiometric mass percent of Zinc and Oxygen are 73.39% and 26.61% respectively (Fig. 5a and Fig. 5b).

TEM and SAED Pattern

TEM is employed to determine the morphology, topography, shape and size of NPs. The ZnO NPs were

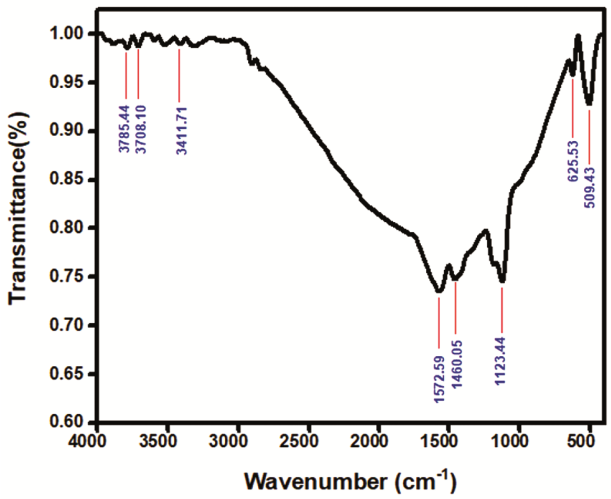

Fig. 4 — FT-IR spectra of plant mediated ZnO NPs

predominantly spherical in shape. The size of the synthesized ZnO NPs was in the range 40–100 nm. The average particle size of sphere-shaped ZnO NPs was 59.08 nm (Fig. 6a). The selected area electron diffraction (SAED) pattern of ZnO NPs prepared by *T. peruviana* flowers extract is given in Fig. 6B. The typical characteristic SAED pattern with bright circular rings characteristic to the indexing planes of (100), (002), (101), (102), (103), (200), and (112) was found which indicated the highly crystalline nature of green synthesized ZnO NPs which is in good agreement with XRD results (Fig. 6b).

Antibacterial activity of ZnO NPs.

Escherichia coli (E.coli) and *S*taphylococcus *aureus* (*S. aureus*) were the two pathogenic drug-resistant bacteria used for checking antibacterial activity of ZnO NPs. Three different concentrations (50, 100, and 200 mg/mL) of ZnO NPs were dissolve in deionized water. 1 mL of different concentration of nanoparticles was added into the well; followed by incubation at 37°C for 24 h. Afterward, Antimicrobial activity of ZnO NPs was assayed by measuring the diameter of the zone of inhibition formed around the well in millimeters. The experiment was done in triplicate, and the average values were calculated for antimicrobial activity. ZnO NPs prepared using *T. peruviana* were found to be more potent against Gram-negative bacteria as compared to Gram positive as shown in Fig. 7 and results were shown in Table 1. Gram-negative bacteria, like *Escherichia coli*, are encased in a layer of lipopolysaccharides (~1–3 µm thick) and peptidoglycans (~8 nm thick), which may facilitate the entry of released ions from nanoparticles (NPs) into the cell. Conversely, Gram-positive bacteria such as *Staphylococcus aureus* have a much thicker peptidoglycan layer, spanning over 80 nm, with covalently attached teichoic and teichuronic acids. The physical interaction between NPs and the cell wall leads to cell wall destruction, which is more detrimental for Gram-negative bacteria due to their thinner peptidoglycan layer compared to Gram-positive bacteria, which potentially acts as a protective barrier[38].

The catalytic activity of ZnO NPs in the synthesis of xanthenes

After characterization of the ZnO NPs, their potential as heterogeneous catalysts was tested in the synthesis of xanthene derivatives *via* condensation

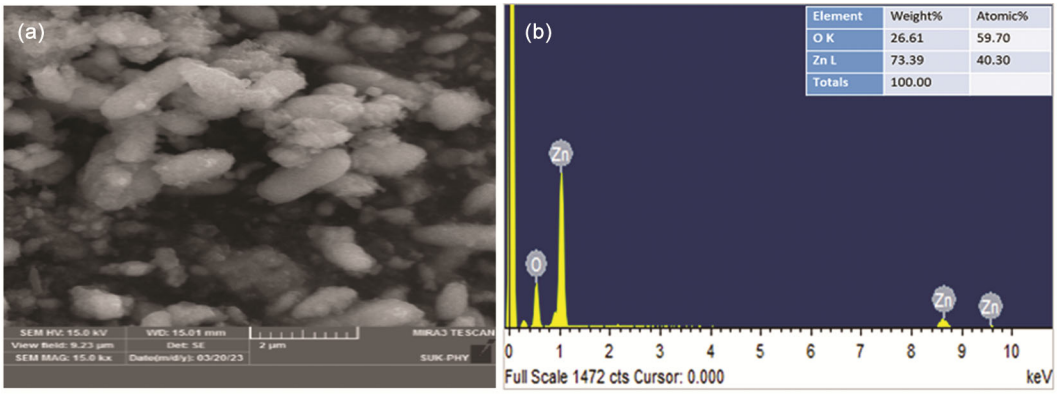

Fig. 5 — (a) FE-SEM image and (b) EDX spectrum of ZnO NPs

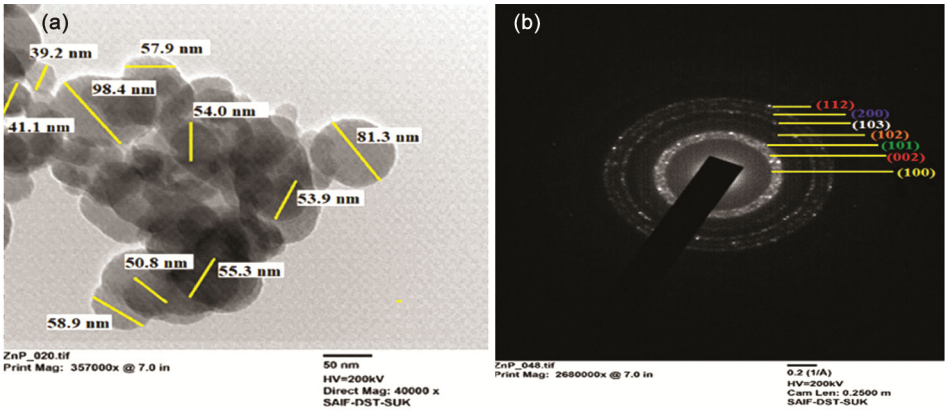

Fig. 6 — (a) HR-TEM and (b) SAED pattern of green synthesized ZnO NPs

reaction. The model reaction was performed in an oven-dried Schlenk flask equipped with a magnetic stir bar. The flask was charged with benzaldehyde (1.0 mmol), dimedone (2.0 mmol), and 25 mol% ZnO nanocatalyst in water:ethanol (90:10) solvent system. The reaction mixture was stirred at RT under standard conditions (Scheme 1). The completion of reaction confirming by TLC [Petrolium ether:ethyl acetate (7:3)] analysis. The reaction mixture was subjected to extraction using ethyl acetate (3×5.0 mL). The product was washed several times with water to afford pure product. The structure of organic product was confirmed by the analysis of using varied spectral techniques including ^{1}H, ^{13}C NMR and mass spectra. Utilizing a nano-sized ZnO nanocatalyst, we obtained a high reaction yield of 98% within 30 min. (Table 2, entry 3a).

The addition of ZnO NPs reduced the reaction time, but produced the low yields. Thus, the reaction was examined with different ZnO NPs concentrations

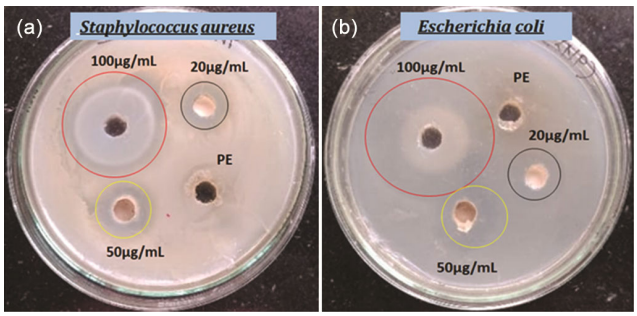

Fig. 7 — Zone of inhibition (mm) a) *Stapylococcus aureus* b) *Escherichia coli*

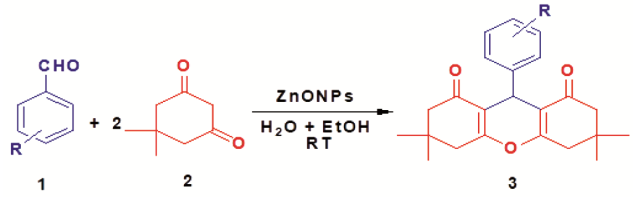

Scheme 1— ZnO nanoparticle catalyzed green synthesis of xanthene

Table 1 — Antibacterial activity of biosynthesized ZnO NPs against Gram-positive and Gram-negative bacteria

Name of Pathogens	Zone of inhibition (mm)	
	PE	Concentration of ZnO NPs 20µg/mL 50µg/mL 100µg/mL
(a) *Staphylococcus aureus* (Gram- Positive)	+ve	18.2 ±1 20.4±1 40.1±2
(b) *Escherichia coli* (Gram-Negative)	–ve	20.7±2 22.1±2 45.2±1

Table 2 — Synthesis of xanthene derivatives using ZnO NPs at RT

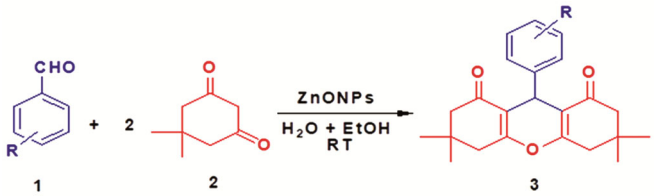

Entry	R-C_6H_4CHO	Product	Time (min)	Yield[b] (%)	Melting Point°C	
					Found	Reported [Ref]
1	C_6H_5CHO	3a	30	96	206-208	205-206[39]
2	4-$NO_2C_6H_4CHO$	3b	35	90	270-272	169-171[40]
3	4-OHC_6H_4CHO	3c	25	85	244-246	245-247[41]
4	4-FC_6H_4CHO	3d	35	80	222-224	221-225[39]
5	4-BrC_6H_4CHO	3e	30	89	236-238	238-240[39]
6	2-BrC_6H_4CHO	3f	40	88	226-228	225–227[40]
7	4-$OCH_3C_6H_4CHO$	3g	25	92	244-246	245-246[39]
8	4-OH,3-$CH_3OC_6H_3CHO$	3h	35	90	222-224	225-227[41]
9	3,4-$CH_3OC_6H_3CHO$	3i	45	89	202-204	200-202[39]
10	2-$NO_2C_6H_4CHO$	3j	5 0	80	232-234	230–238[40]
11	4-ClC_6H_4CHO	3k	60	91	228-230	227–229[40]
12	4-$CH_3C_6H_4CHO$	3l	30	94	224-226	222-224[39]
13	2-Cl C_6H_4CHO	3m	20	89	224-226	223–225[40]
14	3-$CH_3C_6H_4CHO$	3n	45	85	206-208	208-210[39]
15	3-IC_6H_4CHO	3o	40	80	175-176	276-278[39]
16	2-$OCH_3C_6H_4CHO$	3p	35	78	194-195	195–198[40]
17	3- $OCH_2C_6H_5C_6H_4CHO$	3q	25	98	170-172	Present Work

Reaction condition: Benzaldehyde (1 mmol), dimedone (2 mmol), ZnO nanocatalyst 25 mol %, water-ethanol (4:1) 5 mL, RT [b]Isolated yield

to compare their efficacy in getting better yields of xanthene in shorter reaction times. An increase in the quantity of catalyst from 15 to 25 mol % not only decreased the reaction time from one to half hour but also increased the product yield from 85% to 96%. This showed that the catalyst concentration plays a major role in the optimization of the product yield (Table 3). The use of 30 mol % of catalyst decreased the yield of the product to 85%. The higher amount 30 mol % ZnO NPs might have hindered the creation of active catalytic sites thus 25 mol % catalyst facilitated completing the reaction in excellent yields and shorter reaction time. Thus it is the suitable choice for the optimum yield of xanthene. Further, to examine the efficacy of 25 mol % ZnO NPs as catalyst, a series of reactions were conducted using different substituted aldehydes under optimized condition (Table 2).

A plausible mechanism for the synthesis xanthene derivatives in the presence of ZnO NPs is proposed in Scheme 2. Firstly, the ZnO NPs bind with oxygen of carbonyl group; hence it increases the carbonyl activity which in turn makes alpha hydrogen very acidic thereby facilitating the enolization and nucleophilic attack to the aromatic aldehydes leading to the formation of knoevenagel product. Then the knoevenagel product reacted in Michael fashion with another molecule of C–H active molecule and furnished intermediate and cyclization offered the desired product.

Table 3 — Optimization of the reaction conditions

Entry	Catalyst loading (mol%)	Temperature (°C)	Solvent	Time (min)	Yield[b] (%)
1	10	70	Ethanol	76	70
2	15	RT	Ethanol	60	85
3	20	RT	Ethanol	40	88
4	20	80	Ethanol + Ethanol (80:20)	40	88
5	25	80	Water + Ethanol (80:20)	30	94
6	25	RT	Water + Ethanol (90:10)	30	96
7	30	RT	Water + Ethanol (90:10)	35	85

Reaction condition: Benzaldehyde (1.0 mmol), dimedone (2.0 mmol), ZnO nanocatalyst 25 mol %, water-ethanol (4:1) 5 mL, RT [b]Isolated yield

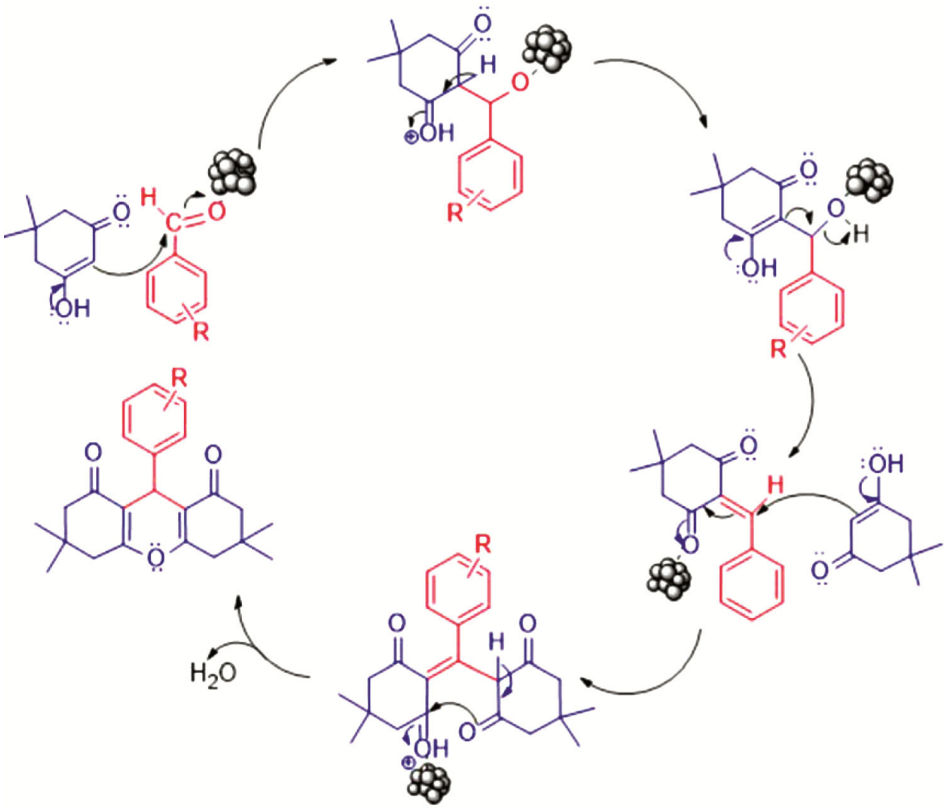

Scheme 2 — Plausible mechanism for the synthesis of xanthene derivatives

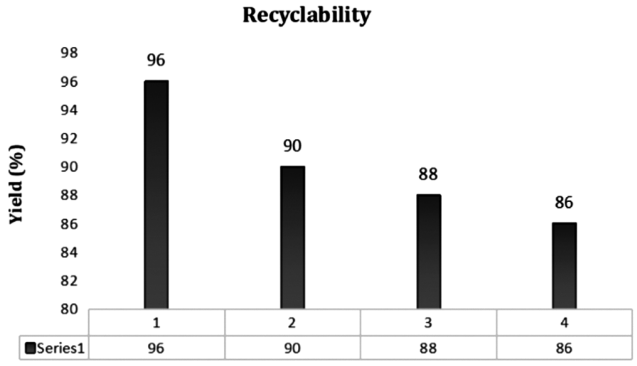

Fig. 8 — Recyclability of green synthesized ZnO NPs

Reusability and reusability study of ZnO NPs

The reusability of the catalyst was also studied under the optimized reaction conditions. After completion of the reaction the catalyst was recovered, filtered and washed repeatedly with ethyl acetate and dried. It was reused under the optimized reaction conditions and it was found that the % yield of xanthene derivatives was negligibly lowered even after five cycles. The catalyst recovered after the first cycle was used for the subsequent four cycles and the yield of the corresponding product obtained in each cycle is summarized in Fig. 8. These observations suggest that the catalyst surface remains active during successive cycles. Although the slight decrease in the catalytic activity of ZnO NPs might be due to the deactivation of the active sites of the catalyst.

Conclusion

The *Thevetia peruviana* (*T. peruviana*) flower extract mediated synthesis of ZnO nanosphere was successfully achieved without the use of any supplementary stabilizing agent or surfactant. Its structure was fully characterized by XRD, UV-Vis, FT-IR, FE-SEM, EDS, and HR-TEM and SAED analysis. Utilizing UV-vis spectroscopy, we conducted an optical investigation to explore into the inherent properties of ZnONPs. The XRD analysis results elucidated that green synthesized ZnO NPs was crystalline in nature. Additionally the morphological characteristics of the ZnO NPs were investigated through FE-SEM and HR-TEM imaging, revealing a spherical structure that aligns with previous studies.

The resulting ZnO nanospheres exhibit potential applications in the field heterogeneous catalysis.

The as-prepared ZnO NPs served as a highly effective heterogeneous solid acid catalyst in the synthesis of xanthene derivatives under environmentally friendly conditions. The eco-friendly catalytic system utilizes non-toxic reagents, short reaction time, excellent yields, and avoidance of harmful organic solvents, and by-products. Additionally, the system's recyclability and straightforward workup procedures, facilitated by the heterogeneous nanocatalyst, enhance its overall environmental acceptability. Using bioprepared ZnO NPs, antibacterial activity was determined based on their incredible potency. The pathogenic drug-resistant bacteria including *E. coli* and *S. aureus* were used in the experiment. The biosynthesized ZnO NPs were found to be more potent against Gram-positive bacteria as compared to Gram-negative bacteria.

Supplementary Information

Supplementary information is available in the website https://nopr.niscpr.res.in/handle/123456789/58776.

Conflict of Interest

The authors declare that they have no competing financial interests or personal relationships that might have influenced the work presented in this paper.

Ethical Approval

The authors declare that the research process did not involve any human or animal experiments.

Acknowledgment

Author Ms. N. P. Patil expresses sincere thanks to Chhatrapati Shahu Maharaj Research, Training and Human Development Institute [SARTHI] (Grant number: CSMNRF/2021/2021-2022/896) for financial support.

References

1 Ramsden J & Andrew W, *Nanotechnology: An Introduction*, (Elsevier Inc., UK) 2016.
2 Albrecht M A, Evans C W & Raston C L, *Green Chem*, 8 (2006) 417.
3 *Considering Whether an FDA-Regulated Product Involves the Application of Nanotechnology*, (Federal Drug Administration, USA), 2014.
4 Ijaz I Gilani E, Nazir A & Bukhari A, *Green Chem Lett Rev*, 13 (2020) 223.
5 Baig N, Kammakakam I & Falath W, *Mat Adv*, 2 (2021) 1821.
6 Szczyglewska P, Feliczak-Guzik A & Nowak, I, *Molecules*, 28 (2023) 4932.
7 Carrapiço A, Martins M R, Caldeira A T, Mirão J & Dias L, *Microorganisms*, 11 (2023) 378.
8 Mittal A K, Chisti Y & Banerjee U C, *Biotech Adv*, 31 (2013) 346.
9 Saravanan A, Senthil Kumar P, Karishma S, Dai-Viet N, Jeevanantham S & Yaashikaa P R, *Cynt Susan George Chemo*, 264 (2021) 128580

10 Duan H, Wang D & Li Y, *Chem Soc Rev*, 44 (2015) 5778.
11 Ovais M, Khalil A T, Islam N U, Ahmad I, Ayaz M, Saravanan M, Shinwari Z K & Mukherjee S, A*ppl Microbio Biotech*, 102 (2018) 6799.
12 Ahmed S, Annu, Chaudhry S A & Ikram S, *J Photochem Photobio B: Bio*, 166 (2017) 272.
13 Matinise N, Fuku X G, Kaviyarasu K, Mayedwa N & Maaza M, *Appl Surf Sci*, 406 (2017) 339.
14 Barzinjy A A, Hamad S M, Abdulrahman A F, Biro S J & Ghafor A A, *Curr Org Synth*, 17 (2020) 558.
15 Vishnukumar P, Vivekanandhan S, Misra M & Mohanty A K, *Mater Sci Semicon Proc*, 80 (2018) 143.
16 Basnet P, Chanu T I, Samanta D & Chatterjee S J, *Photoch Photobio B: Bio*, 183 (2018) 201
17 Xu L, Liang Hai-Wei, Yang Y & Yu Shu-Hong, *Chem Rev*, 118 (2018) 3209.
18 Ndolomingo M J, Bingwa N & Meijboom R, *J Mat Sci*, 55 (2020) 6195.
19 Anastas P & Eghbali N, *Chem Soc Rev*, 39 (2010) 301.
20 Meena S, Kumar K, Saini S, Dandia A & Parewa V, *Adv Nanocat Org Synt Elect*, (2022) 172-192.
21 Nasrollahzadeh M, Mahmoudi-Gom Yek S, Motahharifar N & Gorab M G, *Chem Rec*, 19 (2019) 2436.
22 Hatamie A, Khan A, Golabi M, Turner A P, Beni V, Mak W C, Sadollahkhani A, Alnoor H, Zargar B & Bano S, *Langmuir*, 31 (2015) 10913.
23 Eriksson J, Khranovskyy V, Söderlind F, Käll Per-Olov, Yakimova R & Spetz A L, *Sensors and Actuators B: Chemical*, 137 (2009) 94.
24 Alhujaily M, Albukhaty S, Yusuf M, Mohammed Mustafa K A, Sulaiman G M, Al-Karagoly H, Alyamani A A, Albaqami J & AlMalki F A, Bioengineering, 9 (2022) 541.
25 Ilangovan A, Anandhan K, Prasad K M, Vijayakumar P, Renganathan R, Ananth D A & Sivasudha T, *Med Chem Res*, 24 (2015) 344.
26 Spatafora C, Barresi V, Bhusainahalli V M, Di Micco S, Musso N, Riccio R, Bifulco G, Condorelli D & Tringali C, *Org Biomol Chem*, 12 (2014) 2686.
27 Kumar A, Rout L, Achary L S K, Dhaka R S & Dash P, *Sci Rep*, 7 (2017) 42975.
28 Hafez H N, Hegab M I, Ahmed-Farag I S & El-Gazzar A B A, *Bioorg Med Chem Lett*, 18 (2008) 4538–4543
29 Kushwaha P, Tripathi A K, Gupta S, Kothari P, Upadhyay A, Ahmad N, Sharma T, Siddiqi M I, Trivedi R & Sashidhara K V, *Eur J Med Chem*, 156 (2018) 103.
30 Khurana J M, Magoo D, Aggarwal K, Aggarwal, Kumar R & Srivastava C, *Eur J Med Chem*, 58 (2012) 470.
31 Kantevari S, Bantu R & Nagarapu L, *J Mol Cat A Chem*, 269 (2007) 53.
32 Ghahsare A G, Nazifi Zahra S & Nazifi S M R, *Curr Org Synth*, 16 (2019) 1071.
33 Chibale K, Visser M, Schalkwyk D, Smith P J, Saravanamuthu A & Fairlamb A H, *Tetrahedron*, 59 (2003) 2289.
34 Vijayaraghavan K, Ashokkumar T, *J Env Chem Eng Sci Dir*, 5 (2017) 4866.
35 Ahmad T, Hamid A T, Sharma A & Bhardwaj U, *Int J Adv Res*, 5 (2017) 486.
36 Perez C, Paul M & Bazerque P, *Acta Biol Med Exp*, 15 (1990) 113.
37 Shanavas S, Priyadharsan A, Karthikeyan S, Dharmaboopathi K & Ragavan V, *Mat Today Proc*, 26 (2020) 3531.
38 Yael N S, Asnis J, Urs O, Häfeli & Bach H, *J Nanobiotech*, 15 (2017) 65.
39 Mashooq A B, Ahmed M, Naglah, Ansari S A, Hanaa M, Al-Tuwajiria, Abdullah Al-Dhfyan, *Molecules*, 26 (2021) 3667.
40 Zahra A P, Mohammad M H, Ali E, 40 (2020) 1510.
41 Dhakshanamurthy T, Gajalakshmi S, Res *Chem Intermed*, 46 (2020) 2657.